Catalysis Science & Technology

PAPER

View Article Online
View Journal | View Issue

CrossMark click for updates

Cite this: *Catal. Sci. Technol.*, 2014, **4**, 4366

Evidence for geometric effects in neopentane conversion on PdAu catalysts

David J. Childers,[a] Neil M. Schweitzer,[b] Seyed Mehdi Kamali Shahri,[c] Robert M. Rioux,[c] Jeffrey T. Miller*[d] and Randall J. Meyer*[a]

Received 1st July 2014,
Accepted 5th August 2014

DOI: 10.1039/c4cy00846d

www.rsc.org/catalysis

Silica-supported Pd and shell/core PdAu nanoparticles of a similar size were evaluated for neopentane conversion. Monometallic Pd exhibited poor neopentane isomerization selectivity in favor of high selectivity to primary and secondary hydrogenolysis products. Similarly sized PdAu catalysts of increasing Pd weight loading were synthesized to evaluate the effect of increasing Pd monolayers on neopentane conversion. All PdAu catalysts had neopentane conversion selectivity within the range of monometallic Pd catalysts from previous work (~5–30%). However, there was an inverse relationship between Pd weight loading and neopentane isomerization selectivity. The increase in isomerization selectivity did not correlate to a decrease in heats of adsorption as seen with monometallic Pd catalysts, but was correlated with the catalyst surface structure which suggests a geometric effect as the cause for changes in catalytic performance rather than an electronic effect.

1. Introduction

Bimetallic catalysts often have selectivities and activities that differ significantly from what would be expected from physical mixtures of the two metals.[1–7] Alloying allows the surface structure and composition to become tunable parameters of the catalyst that are able to promote activity or selectivity to desired products. Both ligand (electronic) effects and ensemble (geometric) effects may be responsible for changes in reactivity observed with alloys, but it is difficult to determine experimentally which factor is dominant since it is a challenge to isolate these effects. Electronic effects are manifested as changes in the strength of surface–adsorbate interactions due to modification of the electronic structure when the two metals are alloyed. Ensemble effects arise when reactions require a particular number or arrangement of atoms to form an active site.[6] Understanding the role of electronic and geometric effects in alloy catalysts is complicated because the two effects are often intertwined. Hammer and Norskov have interpreted changes in reactivity of d-band transition metals through the use of a single descriptor: the d-band center of the metal. Adsorption of simple molecules can be directly correlated to the d-band center and enable an understanding of the observed catalytic activity. Through DFT simulations, Hammer and Norskov separated coordination and strain effects from ligand effects in their studies of bimetallic systems and demonstrated for a given adsorption geometry linear correlations exist between the adsorbate binding energy and the position of the d-band center.[8,9] Greeley and Norskov demonstrated this simple d-band correlation held for a large variety of alloys in their study of oxygen adsorption.[10] Experimentally separating the influence of electronic and geometric effects in alloys is a difficult task as the presence of a second metal not only contributes a ligand effect from the change in hybridization between neighboring metal atoms, but strain effects are often introduced due to changes in metal–metal bond distances.[11] In addition, the presence of the second metal may change the type of available sites at the surface (an ensemble effect).

We previously demonstrated the selectivity to isomerization as opposed to hydrogenolysis in neopentane conversion follows the same type of electronic structure correlation described by Norskov *et al.*, as the selectivity is linearly related to the CO adsorption energy (presumably directly governed by the energy of the d-band center).[12] However, it is not clear if the relationship between isomerization selectivity and the electronic structure extends beyond monometallic systems. PdAu provides an interesting test case for electronic structure correlation since Au has previously been used as a modifier for improved selectivity in hydrocarbon reforming.[4]

PdAu alloy catalysts have been studied for a wide variety of reactions, including oxidation, hydrogen peroxide production, hydrochlorination of acetylene and butadiene selective hydrogenation.[13–18] Several different PdAu structural

[a] *Department of Chemical Engineering, University of Illinois at Chicago, USA. E-mail: rjm@uic.edu*
[b] *Center for Catalysis and Surface Science, Northwestern University, USA*
[c] *Department of Chemical Engineering, The Pennsylvania State University, USA*
[d] *Division of Chemical Sciences and Engineering, Argonne National Laboratory, USA. E-mail: millerjt@anl.gov*

configurations are possible depending on the method of catalyst synthesis and metal loadings. Homogeneous alloys with varying Pd and Au loadings have been synthesized by a number of different methods,[15,17,18] however, segregation of either Au or Pd into core–shell geometry has also been well-documented.[16,19–22] Core–shell nanoparticles with Au-rich shells have been synthesized by sequential deposition and annealing.[20] Pd(shell)/Au(core) nanoparticles has been synthesized through a number of different methods: electro-deposition,[21] colloidal synthesis[16,22] and seeded growth (addition Pd shells to pre-made Au particles).[19] Both Pd and Au have been used as promoters to enhance the catalytic properties of the other by decorating the surface.[23,24] Dolle *et al.* studied the growth of Pd films on Au(110) surfaces; at low Pd coverage (0–0.5 ML), gold preferentially covers Pd atoms, but at higher coverage (0.5 to 3 ML), the growth of Pd introduces a small tensile strain due to the match with the Au lattice until ~9 ML when the lattice parameter of the Pd lattice relaxes significantly.[25] Li *et al.* performed experiments on PdAu surfaces and found at low palladium coverage, the surface restructures to form low-coordination gold ensembles that block atop sites on palladium.[26] At high palladium coverage, CO adsorbs on bridge sites, similar to pure palladium. Goodman's group has investigated the structure of PdAu single crystal surfaces.[13] The addition of Pd atoms to a Au single crystal surface led to isolation of Pd atoms on the Au surface.[20,27,28] Electronic effects stem from charge transfer from gold to palladium which shifts the d-band center of Pd away from the Fermi level and weakens adsorbate bonding to Pd.[29] This weakened adsorbate bonding results in improved neopentane isomerization selectivity as has been observed in previous work.[12]

A number of theoretical studies have been conducted on PdAu systems to analyze the observed changes in catalytic behavior.[13,26,30–33] Most findings have concluded a combination of geometric and electronic effects contribute to Au altering the behavior of Pd. For example, Neurock *et al.* found that both surface coverage and metal–adsorbate bond strength are influenced by geometric effects, since the surface coverage and bond strength are correlated (bond strength decreases as coverage increases).[34] The bond strength of ethylene to Pd is weakened by the addition of Au which makes the sites more active for ethylene hydrogenation; however, gold also reduces the binding energy of H by 130 kJ mol^{-1} which deters hydrogenation. For ethylene hydrogenation, these two effects balance one another and the result is a negligible effect on activity but there is an effect on initial ethane dehydrogenation selectivity by increasing the barrier for ethylidyne formation by 25 kJ mol^{-1}. Although charge transfer was observed (an electronic effect), it was not significant and was therefore discounted as a cause for the observed change in catalytic behavior. Mazzone *et al.* used density functional theory to study the adsorption of CO on PdAu (111) and (100) surfaces.[29] Isolated Pd atoms on a Au surface induces a local relaxation effect that causes shortened Pd–Au bond distances compared to typical Au–Au bond distances resulting in a stronger Pd–Au bond and weakened CO binding energy by as much as 30 kJ mol^{-1}. Garcia-Mota *et al.* also used DFT to study the adsorption of CO on PdAu surfaces.[35] Their calculations showed that isolation of Pd on Au surfaces is thermodynamically favorable and isolation of Pd was stabilized by the presence of CO at high pressures ($>10^{-2}$ Torr).

Gold has been previously alloyed with Pt group metals to study neopentane conversion. Schwank *et al.* performed neopentane hydrogenolysis over Pt–Au/SiO_2 and Pt–Sn/Al_2O_3 catalysts.[36] Pt–Au samples did not have a significantly different selectivity compared to the monometallic samples. Bonarowska *et al.* used PdAu catalysts to study neopentane conversion.[15] They synthesized two series of samples prepared by direct redox and incipient wetness impregnation. The reported dispersion of ~0.05 implies that the particles were very large (20 nm). The monometallic Pd sample showed a single-point isomerization selectivity of almost 40% at low conversion (<1%), about a 15% increase from the selectivity found in previous work.[12] PdAu catalysts with lower Au content (0.05–0.20 wt.%) showed either no change or a slight decrease in isomerization selectivity whereas at a loading of 0.40 wt.% Au, the isomerization selectivity increased to almost 50% indicating a positive effect on selectivity.

Here we report on the synthesis, characterization and testing of four PdAu catalysts supported on silica with different Pd loadings. The physical and chemical effects of alloying palladium with gold was investigated by electron microscopy, X-ray energy dispersive spectroscopy, diffuse-reflectance Fourier transform spectroscopy (DRIFTS), extended X-ray absorption fine structure (EXAFS), chemisorption and adsorption calorimetry of CO. Neopentane hydrogenolysis was the probe reaction used to evaluate changes in catalytic performance of Pd upon alloying with Au.

2.0 Experimental methods

2.1 Catalyst synthesis

All samples were synthesized using sequential impregnation of Au then Pd on silica (Davisil A60 silica gel from Sigma-Aldrich, 200 m^2 g^{-1} and 1.15 mL g^{-1} pore volume) using both incipient wetness impregnation (IWI) and strong electrostatic adsorption (SEA).[37] During IWI, a support is contacted with just enough metal-precursor solution to fill the pore volume. All of the metal precursor solution contacts the surface due to the incipient amount of liquid used; however, this synthetic method typically leads to significant particle growth during drying and pretreatment. In contrast, SEA uses an excess amount of solution with a controlled pH to favor the uptake of the metal precursor. The SEA method requires an appropriately charged metal precursor based on the point of zero charge (PZC) of an oxide support and the pH of the solution. The hydroxyl groups on the surface of the oxide support will protonate or deprotonate depending on the pH of the solution relative to the PZC of the support. Precursors can then be selected that have the opposite charge as the

support at a certain pH value and so the electrostatic interaction between the support and the precursor leads to adsorption of the metal precursor to the surface.[37] Weight loadings were chosen to create catalysts with approximately one monolayer of Pd increasing to 4 Pd monolayers on the Au particle surface. An estimate of the number of Pd monolayers was determined assuming that one Pd atom covers a single Au atom on the surface and Pd disperses uniformly on the surface of the Au nanoparticles. Post treatment steps were evaluated using EXAFS and XANES spectra to confirm reduction of the metal.

0.52% Pd–3% Au & 1% Pd–3% Au. Gold was added to silica using the SEA method. Silica (35 g) was added to an ammonia solution (NH_4OH (5 mL)/H_2O (200 mL)). 1.7 g of $HAuCl_4$ was added to 50 mL of H_2O, 2.5 mL ethylenediamine and 5 mL of NH_4OH which resulted in a dark orange-yellow solution with a pH of 11. These solutions were combined and stirred for 10 min. followed by vacuum filtering of the solid catalyst, which was subsequently washed 3 times with H_2O. The sample was dried in a vacuum oven overnight at 50 °C. The sample was treated in flowing 4% H_2/He at 150 °C. For the 0.52% Pd sample, 0.55 g of 10% $Pd(NH_3)_4(NO_3)_2$ solution was then added to 5 g of Au/SiO_2 using IWI and dried at 125 °C overnight and treated in flowing O_2 at 225 °C for 3 h and reduced at 200 °C. For the 1% Pd sample, 1.42 g of 10% $Pd(NH_3)_4(NO_3)_2$ was added to 1 mL NH_4OH and 2.5 mL H_2O solution and then added dropwise to 5 g of Au/SiO_2. The sample was dried at 125 °C overnight followed by treatment in flowing O_2 at 225 °C for 3 h and treated in flowing H_2 at 200 °C for 30 min.

2% Pd–3.5% Au & 4% Pd–3.5% Au. Gold was added to silica using the same SEA method described above. The sample was dried in an oven overnight at 90 °C. The sample was treated at 150 °C in 4% H_2/He. For the 2% Pd sample, 2.78 g of 10% $Pd(NH_3)_4(NO_3)_2$ aqueous solution was added to an ammonia solution (NH_4OH (1 mL)/H_2O (4 mL)) to achieve a pH of 11 and then added dropwise to 5 g of Au/SiO_2. The sample was dried at 100 °C overnight and treated in flowing O_2 at 225 °C for 3 h and treated in flowing H_2 at 225 °C for 30 min. For the 4% Pd sample, the addition of Pd was done in two steps. Initially, 2.84 g of 10% $Pd(NH_3)_4(NO_3)_2$ was dropwise to a solution of NH_4OH (1 mL) and H_2O (4 mL) and 5 g of Au/SiO_2. The sample was dried at 100 °C overnight and then 2.75 g of precursor was added dropwise to an ammonia solution (NH_4OH (1 mL)/H_2O (4 mL)). The sample was again dried overnight at 100 °C and then treated in flowing O_2 at 225 °C for 3 h and treated in flowing H_2 at 225 °C for 30 min.

2.2 STEM and X-ray Energy Dispersive Spectroscopy (XEDS)

The STEM spectra were obtained at UIC's Research Resources Center Facility using the JEOL-ARM 200CF aberration corrected microscope (70 pm spatial resolution and 300 meV energy resolution). Samples were dispersed in isopropyl alcohol and sonicated for 20 min. A drop of the solution was added to a holey-carbon copper grid and dried under a heat lamp for 20 min. Images were taken using the High Angle Angular Dark Field (HAADF) mode. XEDS measurements were collected using an Oxford Instrument X-Max 80 mm^2 SDD detector. A 1.3 Å probe size with a 143 pA beam current was used to measure line scan data with a 1 s dwell time per step. Data was plotted using the Oxford Instrument Aztec program.

2.3 Extended X-ray Absorption Fine-Structure Spectroscopy (EXAFS)

X-ray absorption spectroscopy (XAS) measurements at the Pd K (24 350 eV), and Au L_3 (11 919 eV) edges were made on the bending magnet beamline of the Materials Research Collaborative Access Team (MRCAT) at the Advanced Photon Source (APS) at Argonne National Laboratory. Measurements were made in transmission mode. A palladium or gold foil spectrum was acquired through a third ion chamber simultaneously with each measurement for energy calibration.

Samples were prepared by grinding the catalysts into a fine powder and pressing them into a metal cylinder sample holder capable of holding up to six individual samples. The sample holder is then placed in a quartz tube with ports on each end to flow gases or isolate the sample after treatment. The sample thickness was chosen to give a total absorbance at the Au L_3 or Pd K edge between 1–2 absorption lengths and edge steps around 0.3–0.5. Samples were reduced at 300 °C in 4% H_2/He mixture (50 cm^3 min^{-1}) at atmospheric pressure. After reduction, the samples were purged with He (100 cm^3 min^{-1}) and cooled to room temperature in He flow. Trace oxidants in He were removed by passing through a Matheson PUR-Gas Triple Purifier Cartridge containing a Cu trap. All EXAFS spectra were obtained at room temperature in He.

2.4 Neopentane hydrogenolysis and isomerization

Neopentane hydrogenolysis and isomerization was studied using 0.05–0.15 grams of catalyst diluted with 0.9 grams of silica and loaded into a 0.5" O.D. quartz plug flow reactor. Glass wool was used for the bottom 2 cm of the bed. A 0.5 cm long layer of silica was placed on top of the glass wool, followed by the catalyst–silica mixture resulting in an overall catalyst bed height of 3 cm. The reactor was purged with He for 5 min before each run, and the catalyst was reduced in 4% H_2/He as the temperature was increased to the reaction temperature, 271 ± 2 °C. A K-type thermocouple was inserted from the bottom of the reactor into the lower portion of the catalyst bed. Once the reaction temperature stabilized, the pre-mixed reactant feed gas consisting of 0.35% neopentane and 3.5% H_2 balanced in He was passed through the reactor. The flow rate of the feed gas was varied from 25 to 100 cm^3 min^{-1} to obtain differential conversions (1–4%). Although the selectivity does not change drastically with conversion, the selectivities reported are those obtained by extrapolation to zero conversion.[12] Each flow rate was run for at least one hour to ensure steady-state conversion had been reached. An Agilent 6890 N gas chromatograph (using a

J&W Scientific GS-Alumina column) with an FID detector was used to analyze the products and was equipped with a back pressure regulator on the outlet to maintain the system at a constant pressure of 9 psig. Each experimental run was completed within six hours for consistency and multiple runs for each catalyst were performed. No appreciable deactivation was observed in any of the catalysts over this period of time. The maximum error of any selectivity measurements was 6%, with most of the data being reproducible within 2%. Turnover rates were calculated based upon the number of active sites determined by the dispersion measured by CO chemisorption to account for the fact that surface Au sites do not adsorb CO at the experimental conditions employed and are not active for neopentane conversion.[38–40]

2.5 Diffuse Reflectance Infrared Fourier Transform Spectroscopy (DRIFTS)

Infrared spectra were obtained using a Thermo Scientific Nicolet 6700 FTIR spectrometer equipped with a Harrick Scientific Praying Mantis diffuse reflectance *in situ* cell at the Northwestern Clean Catalysis (CleanCat) Core Facility. Samples were ground to a fine powder using a mortar and pestle, and packed into the sample chamber to create a uniform surface. The chamber was purged with Ar, and then the gas was switched to 10% H_2/N_2 and the temperature was raised to 250 °C and held for 15 min. After reduction of the catalyst, the gas was switched back to Ar and the temperature was reduced to 25 °C. A background scan was then recorded, which was averaged over 100 scans (2 minute observation time) with 4 cm^{-1} resolution. The sample was then exposed to 1.02% CO/N_2 and another scan was taken once equilibrium was reached, at which point the flow was changed back to Ar and a final scan was taken once the intensity of the adsorbed CO peak was invariant with time. The linear-to-bridge bound ratio reported here do not take into account the differences in extinction coefficients between the adsorption sites and therefore are not quantitative, but do reflect qualitative differences between catalysts.[41]

2.6 CO chemisorption

The CO chemisorption measurements were conducted at the Northwestern University Clean Catalysis (CleanCat) Core Facility using an Altamira Instruments AMI-200. Catalysts (0.05–0.2 g) were loaded into a U-shaped quartz reactor tube, which was weighed before and after sample addition to ensure an accurate weight measurement. The loaded tube was then mounted in the furnace and the catalysts were reduced in 4% H_2/Ar at 300 °C for 2 h (10 °C min^{-1} ramp rate) and then flushed for 30 min in He. Using a six-way valve, 5% CO/He was then pulsed (595 μL loop volume) into the system 15 times at 30 °C to ensure the surface was saturated. Each pulse peak was integrated to find the volume of CO remaining following adsorption. Surface saturation was typically reached within 10 pulses. The dispersion determined by CO chemisorption included the average stoichiometric factor determined from the DRIFTS linear-to-bridging ratios for each catalyst. Linear bound CO accounts for one CO molecule per surface atom while bridge bound CO implies there is one CO molecule per two surface atoms. The equation used to determine the dispersion of Pd in the $PdAu/SiO_2$ catalysts is given below.

$$\text{Dispersion} = \frac{\text{mol CO adsorbed}}{\text{mol metal}} \times \big((\text{linear CO fraction} \times 1) + (\text{bridge CO fraction} \times 2)\big)$$

2.7 CO heats of adsorption

Determination of the initial heat of adsorption of carbon monoxide on the monometallic Pd/SiO_2 and four $PdAu/SiO_2$ catalysts (60–70 mg) was conducted utilizing a Setaram Sensys EVO differential scanning calorimetry interfaced with a plug-flow reactor. The plug-flow reactor was connected to a mass spectrometer. After reduction at 300 °C in 5.11% H_2/Ar (both gases 99.999%) for 2 h, the catalyst was cooled down to 35 °C in the same gas. The catalyst was exposed to a mixture of 1% CO (99.999% research grade) in He (99.9999%, research grade) pulsed into the 5% H_2/Ar stream from a ten-way switching value with a 1000 μL sample loop. The number of moles of CO per pulse calculated from the ideal gas law was ~4×10^{-4} mmol. Twenty pulses of carbon monoxide were employed; the initial heat of adsorption was determined by only considering injections in which the entire pulse of carbon monoxide was consumed. The number of pulses completely consumed depended on the content of Pd in the catalyst.

3.0 Results

3.1 Particle size analysis

STEM imaging was used to determine particle size. A representative STEM image for the 2% Pd + 3.5% Au catalyst and corresponding size distribution are shown in Fig. 1. Table 1 summarizes the particle sizes for all catalysts determined by both STEM and chemisorption methods. The four catalysts have similar particle sizes. Data for similar sized monometallic Pd catalysts is taken from Childers *et al.* for comparison with PdAu.[12] Particle size has an effect on neopentane selectivity and activity; therefore, in order to isolate the effect of Au alloying, it is critical that catalysts with varying composition have similar particle size.[12]

Fig. 2 shows a line scan and the corresponding STEM image for the 0.52% Pd + 3% Au and 1% Pd + 3% Au catalysts, respectively. Line scans demonstrate an increased concentration of Pd on the outer shells of the nanoparticles while the Au is concentrated within the core. Analysis performed on several particles per catalyst sample confirmed that a majority of the nanoparticles have a Au-rich core and Pd-rich shell structure.

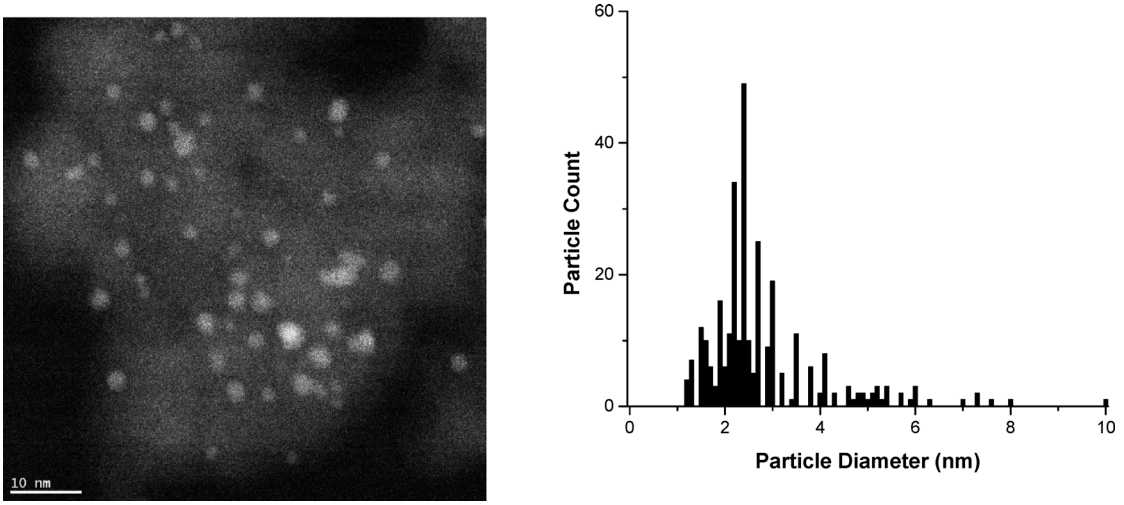

Fig. 1 2% Pd–3.5% Au sample image and particle size distribution determined by STEM.

Table 1 Particle size determined by STEM and CO chemisorption

Sample	Particle size by STEM (nm)	Particle size by CO chemisorption (nm)
2% Pd_2.5 nm	2.5 ± 1.1	4.3 ± 0.4
2% Pd_3 nm	3.0 ± 0.8	3.8 ± 0.4
0.52% Pd + 3% Au	2.9 ± 1.4	1.7 ± 0.2
1% Pd + 3% Au	2.8 ± 1.2	2.2 ± 0.2
2% Pd + 3.5% Au	3.3 ± 1.1	2.3 ± 0.2
4% Pd + 3.5% Au	4.1 ± 1.0	3.8 ± 0.4

3.2 EXAFS

Extended X-ray absorption fine structure (EXAFS) spectra were collected for each catalyst following reduction at 300 °C and fit to determine bond distances and coordination numbers (CN). The EXAFS spectra for the Pd K-edge and the Au L_3-edge spectra are given in Fig. 3 and the fitting parameters are summarized in Table 2. The reference Pd and Au foil spectra (black dotted lines) are included for comparison. The Pd foil EXAFS in Fig. 3a show two prominent peaks at 1.97 and 2.47 Å with an intensity ratio of 2 : 1, typical of metallic Pd.[42] The PdAu catalysts have small shifts in these peaks to 2.00 and 2.55 Å respectively; however, these shifts are not unexpected due to slight changes in particle size amongst samples. The 4% Pd–3.5% Au catalyst also has the 2 : 1 peak intensity ratio typical of metallic Pd, while the other PdAu catalysts show a change in that ratio to about 1.6 : 1. This change indicates that there are Au atoms in contact with Pd in the catalyst. The Pd–Pd bond distance in all of the catalysts is 2.80 Å, an expansion by 0.05 Å from the metallic bond distance of 2.75 Å.[12] This expansion in the Pd–Pd bond distance could be the result of strain due to the epitaxial growth of Pd over Au.[25] Differences in the coordination number between Pd–Pd and Pd–Au show the majority of the palladium atoms in this catalyst are bonded to other palladium, as would be expected for a core–shell configuration. The fraction of Pd atoms which interact with Au decreases as the palladium loading increases. A Pd–Au bond distance of 2.82 Å is approximately the average of the bulk Pd–Pd and bulk Au–Au bond distances. Fig. 3b shows the Au L_3-edge spectra of all catalysts and the Au foil reference. The Au foil spectra show two peaks at 2.45 and 2.95 Å, and these peaks shift to 2.37 and 3.00 Å in the PdAu catalysts, respectively.[43,44] The spectra show almost no variation from metallic Au except the peak at 2.45 Å is shifted lower by 0.075 Å and the peak at 2.95 Å is shifted higher by 0.025 Å. The fitting parameters in Table 2 show that there are very few Au–Pd interactions and no change to the bulk properties of Au in the bimetallic catalysts. The Au–Au bond distance contraction from 2.88 to 2.86 Å is not unexpected for smaller Au particles.[22] This lack of change indicates that nearly all gold present in the catalysts are surrounded by other gold atoms.

3.3 Diffuse Reflectance Infrared Fourier Transform Spectroscopy (DRIFTS)

Characterization of CO adsorption on the PdAu/SiO_2 catalyst was conducted with DRIFTS to determine changes in CO bonding to the catalyst surface with the addition of increasing amounts of Pd. Peaks in the range of 1800–2000 cm^{-1} are assigned to bridge bound CO; within this range, peaks between 1800 and 1900 cm^{-1} are attributed to CO bound on terrace sites while peaks between 1900 and 2000 cm^{-1} are believed to be due to the presence of CO bound to corner and edge sites.[45,46] The linear bound region can also have two peaks typically occurring around 2080 and 2050 cm^{-1} which Lear *et al.* have assigned to linear bound CO on corner sites and edge sites respectively.[45]

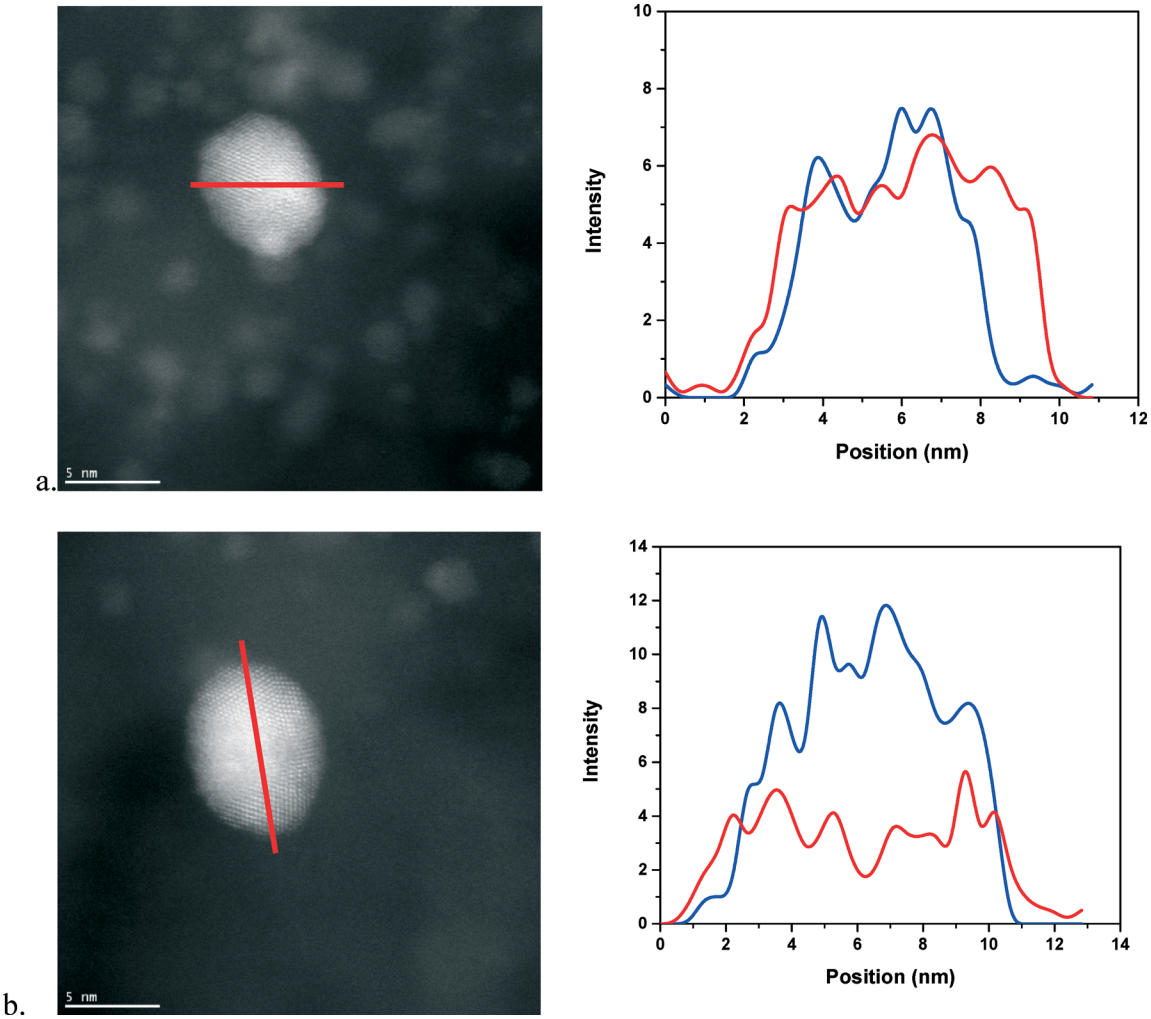

Fig. 2 Linescan data for 0.52% Pd–3% Au catalyst (a) and 1% Pd–3% Au catalyst (b) Pd (red) and Au (blue).

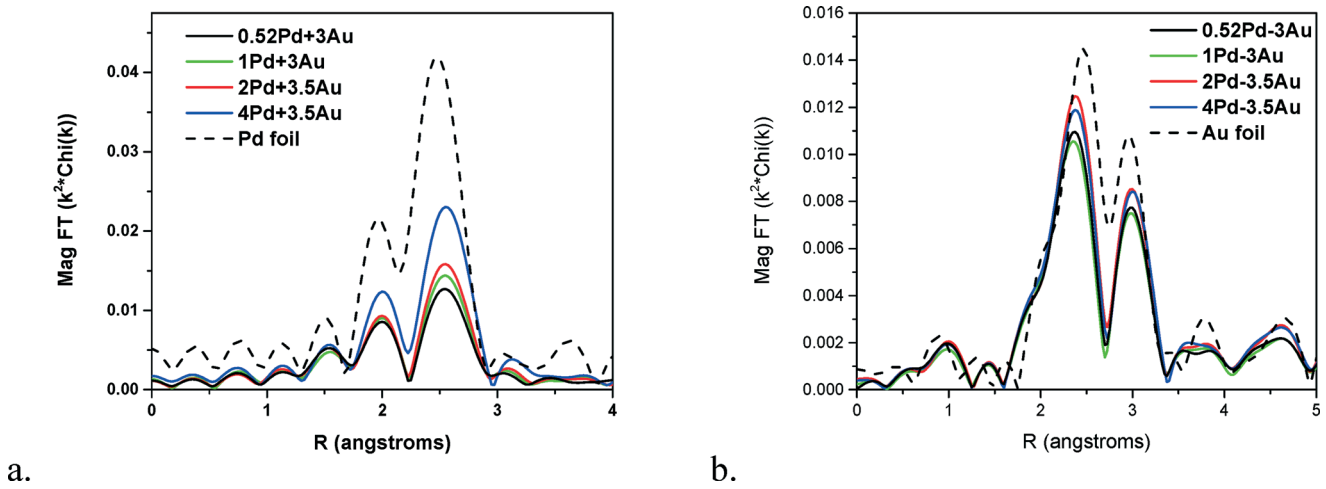

Fig. 3 EXAFS spectra for (a) Pd K-edge and (b) Au L_3-edge.

Fig. 4 shows the DRIFTS spectra for the PdAu catalysts as well as monometallic Pd catalysts with a similar particle size. The linear bound CO peak in each spectrum was normalized to the largest linear peak to facilitate direct comparison amongst catalysts. Palladium is known to typically favor bridge bound CO over linear bound CO and alloying with gold caused

Table 2 EXAFS fitting parameters for Pd K-edge and Au L_3-edge

Catalyst	Pd edge energy (keV)	Scatter	Coordination number	Bond distance (Å)
0.52Pd–3Au	24.350	Pd–Pd	6.2	2.80
		Pd–Au	3.4	2.82
1Pd–3Au	24.350	Pd–Pd	6.4	2.80
		Pd–Au	2.9	2.82
2Pd–3.5Au	24.350	Pd–Pd	7.0	2.80
		Pd–Au	2.6	2.82
4Pd–3.5Au	24.350	Pd–Pd	10.0	2.80
		Pd–Au	1.7	2.82
Catalyst	**Au edge energy (keV)**	**Scatter**	**Coordination number**	**Bond distance (Å)**
0.52Pd–3Au	11.919	Au–Au	10.2	2.86
		Au–Pd	1.1	2.80
1Pd–3Au	11.919	Au–Au	9.8	2.86
		Au–Pd	1.4	2.83
2Pd–3.5Au	11.919	Au–Au	11.2	2.87
		Au–Pd	1.0	2.83
4Pd–3.5Au	11.919	Au–Au	11.3	2.87
		Au–Pd	1.1	2.82

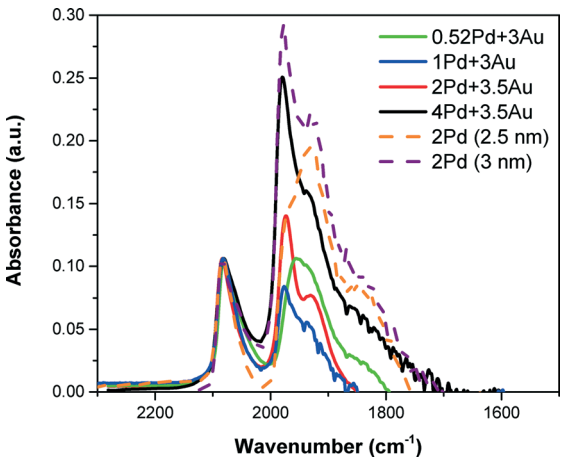

Fig. 4 DRIFTS spectra of the adsorption of carbon monoxide on silica supported PdAu catalysts: 0.52% Pd–3% Au (green), 1% Pd–3% Au (blue), 2% Pd–3.5% Au (red) and 4% Pd–3.5% Au (black) and monometallic Pd catalysts of similar particle size (dotted lines): 2.5 nm (orange) and 3 nm (purple). Intensity of linear bound CO peak at 2082 cm^{-1} normalized for each catalyst for comparison.

an increase in the linear-to-bridge ratio, suggesting division of large Pd ensembles into smaller ones. All catalysts have a peak centered at 2082 cm^{-1} which is attributed to linear bound CO on isolated Pd atoms on the Au–Pd surface.[20,47] CO bound on Au surfaces shows a linear peak around 2110 cm^{-1} which is not seen in any of the catalysts.[17] All catalysts possess a pair of peaks in the bridge bound region that shift peak position depending on the Pd/Au composition. The 0.52% Pd–3% Au catalyst has a peak at 1955 cm^{-1} which is assigned to bridge bound CO on corner and edge sites and another peak at 1860 cm^{-1} which is assigned to bridge bound CO on terrace sites.[14,48,49] These peaks are in the same positions as the monometallic Pd (2.5 nm) catalyst and all other catalysts have two bridge bound peaks centered at 1970 cm^{-1} and 1930 cm^{-1}. Both of these peaks are in the range of bridge bound CO on corners and edges, but Lear *et al.* have further defined these two distinct peaks as bridge bound CO on (100) facets (1970 cm^{-1}) and CO bridge bound on (111) facets (1930 cm^{-1}).[45] These PdAu catalysts have similar peak positions to the monometallic Pd (3 nm) catalyst, except that the bridge bound CO peak on terrace sites is located at 1830 cm^{-1}. All PdAu catalysts lose the bridge bound CO peak on terrace sites centered at 1830 cm^{-1} suggesting that gold breaks up palladium ensembles. The resolution of two distinct peaks in the bridge bound region and the loss of the peak around 1830 cm^{-1} are evidence for bimetallic formation.[20,33,47] The similarity of these spectra to the monometallic Pd spectra suggests that any surface Au present does not adsorb CO. Marx *et al.* found little contribution to the DRIFTS spectra from CO adsorbed on Au sites on Pd/Au alloys.[50]

The linear-to-bridge ratios of adsorbed CO are calculated by comparing the area of the different peaks (Table 3). All PdAu catalysts have a higher linear-to-bridge ratio than monometallic Pd catalysts with similar STEM-determined particle size.[12] Alloying with gold causes a decrease in bridge bound CO, a further indication that palladium ensembles break up. There is no apparent correlation between palladium weight loading and linear-to-bridge ratio as the 1% Pd–3% Au catalyst has the highest ratio. However, the addition of Pd above 1 wt.% loading causes the linear-to-bridge ratio to decrease to a value similar to monometallic Pd catalyst, consistent with the presence of a contiguous overlayer of Pd on the Pd(shell)/Au(core) nanoparticle. The change in the DRIFTS spectra are another indication that palladium is altered by alloying with gold and has been seen in literature.[47,51]

3.4 Calorimetric determination of CO heat of adsorption on PdAu/SiO_2 catalysts

The initial heat of adsorption determined previously for a pair of Pd/SiO_2 catalysts with a mean TEM particle size of

Table 3 Initial heat of CO adsorption values (±10 kJ mol^{-1}) in the presence of chemisorbed hydrogen and linear-to-bridge ratios from DRIFTS

Sample[a]	CO (initial) heat of adsorption on H-covered surface[b] (kJ mol^{-1} CO)	Linear to bridge ratio
2Pd/SiO_2_2.5 nm[c]	92	0.20 : 1
0.52Pd–3Au/SiO_2	104	0.59 : 1
1Pd–3Au/SiO_2	97	0.94 : 1
2Pd–3.5Au/SiO_2	99	0.37 : 1
4Pd–3.5Au/SiO_2	90	0.25 : 1

[a] Catalysts were initially reduced under 5.11% H_2/Ar (both gases, 99.999% UHP) for 2 h at the specified reduction temperature, followed by subsequent cooling in H_2. [b] Initial heat of CO adsorption determined by microcalorimetry on a reduced H-covered Pd or PdAu surface. [c] Catalyst from Ref. 12.

2.5–3 nm was ~130 kJ mol^{-1}.[12] The heat of CO adsorption on Pd was previously determined for the catalysts reduced in H_2, evacuated at the reduction temperature, followed by cooling in vacuum to the adsorption temperature (35 °C). In the previous work, the differential (initial) heat of adsorption was determined using a volumetric adsorption instrument (Micromeritics ASAP 2020C) interfaced with a Setaram Sensys EVO differential scanning calorimeter. For the PdAu catalysts studied in this work, calorimetric measurements of CO were conducted in a plug-flow reactor interfaced to a mass spectrometer using the same Setaram Sensys EVO differential scanning calorimeter. Attempts to measure the heat of adsorption of CO on the PdAu catalysts in an inert environment were unsuccessful due to the large heat flow associated with the oxidation of CO by the oxygen in He (UHP, 99.999%). The heat flow observed calorimetrically was accompanied with a nearly identical change in the CO_2 (44 m/z) signal in the mass spectrometer. All attempts to eliminate the CO oxidation reaction were unsuccessful including utilizing a CO/He mixture containing research grade He (99.9999%). In order to reduce the oxidation of carbon monoxide, we introduced pulses of CO into a 5% H_2/Ar stream. The Ar contained significantly less oxygen than both grades of He. Reduction of the catalyst and cooling down to the adsorption temperature in the H_2/Ar ensured that Pd was covered with chemisorbed hydrogen. Therefore, the CO heat of adsorption values reported in Table 3 are those for H-covered Pd surfaces. Chemisorbed hydrogen will lower the heat of adsorption of CO compared to an adsorbate-free surface of Pd.[52] For the monometallic Pd sample, the heat of adsorption of CO decreased by ~40 kJ mol^{-1} in the presence of chemisorbed H. At this point, we do not know to what extent the potential incorporation of Au in the Pd shell layer influences the energetics of H adsorption, but the reported initial heats of adsorption of CO are approximately the same across all samples demonstrating Pd dominates the interaction with CO.[53–55] The results in Table 3 also show that increasing Pd wt.% decreased the heat of adsorption to a value similar to monometallic Pd.

3.5 Neopentane hydrogenolysis and isomerization

Neopentane conversion was performed at 275 °C, 9 psig and varying flow rates (25–100 cc min^{-1}) in order to maintain differential conversion (1–4%) behavior. Two reaction pathways are possible for this reaction: hydrogenolysis and isomerization. Isomerization products include isopentane (single isomerization) and *n*-pentane if isopentane undergoes isomerization. A single hydrogenolysis step results in the formation of isobutane and methane, and secondary hydrogenolysis reactions produce additional methane and lighter hydrocarbons (propane and ethane). The selectivity values (extrapolated to 0% conversion) and calculated turnover rates (TOR) based on Pd surface concentration determined from CO chemisorption are provided in Table 4. Since the activity of gold is several orders of magnitude lower for neopentane hydrogenolysis than Pd,[38] CO chemisorption is required to determine the surface concentration of palladium for the calculation of nominal turnover rates. Products with non-zero selectivity at 0% conversion are considered primary products while products with 0% selectivity in the limit of 0% conversion are considered secondary or higher order products.[56] The isomerization selectivity is defined as the selectivity to isopentane since no *n*-pentane was observed, and hydrogenolysis products are $<C_5$ molecules.

Table 4 TOR and product selectivity data for PdAu and Pd catalysts

Catalyst	Dispersion[a]	TOR (mol conv/metal site s^{-1})	Initial product distribution (%)					
			CH_4	C_2H_6	C_3H_8	n-C_4H_{10}	i-C_4H_{10}	i-C_5H_{12}
0.52% Pd + 3% Au	0.59	6.2×10^{-4}	38	2	3	0	33	26
1% Pd + 3% Au	0.45	3.0×10^{-4}	43	3	6	0	29	20
2% Pd + 3.5% Au	0.43	5.8×10^{-4}	43	0	4	1	33	19
4% Pd + 3.5% Au	0.26	1.3×10^{-3}	45	0	3	4	36	12
2% Pd/SiO_2_3 nm	0.33	7.7×10^{-4}	40	0	1	1	34	24
2% Pd/SiO_2_2.5 nm	0.40	1.0×10^{-3}	49	1	5	2	33	9

[a] Dispersion determined by CO chemisorption for PdAu catalysts and by STEM for Pd catalysts.

The isomerization selectivity for all of the $PdAu/SiO_2$ catalysts falls within the range of the two monometallic Pd catalysts (Table 4). There is a trend of increasing isomerization selectivity with decreased palladium weight loading. Primary hydrogenolysis (*i.e.*, increase in methane selectivity) increases as the amount of Pd increases in the $PdAu/SiO_2$ catalysts, but the secondary hydrogenolysis product selectivity doesn't show a consistent trend with Pd content in the bimetallic catalysts.

4.0 Discussion

4.1 Explanation of observed activity and selectivity of PdAu alloys

XEDS measurements demonstrated particles had Pd-rich shells and Au-rich cores. EXAFS data revealed palladium in the bimetallic catalysts is under expansive strain compared to monometallic palladium. The data from EXAFS demonstrates the Pd–Pd bond length increases from 2.75 to 2.80 Å when alloyed with Au. This type of lattice expansion has been documented previously for Pd(shell)/Au(core) catalysts.[19,22,57] The activity of the bimetallic catalysts also falls within the monometallic Pd behavior for neopentane hydrogenolysis established in our previous work.[12] Although the selectivity is not significantly improved compared to monometallic palladium, the dependence of the selectivity with the effective particle size has changed. An isomerization selectivity of ~25% requires a monometallic palladium particle of ~3 nm, whereas the 0.52% Pd–3% Au catalyst with comparable isomerization selectivity has an effective particle size of 1.7 nm as determined by CO chemisorption. Dispersion determined by chemisorption is a more relevant determination of the number of active sites than STEM since Au has an almost negligible neopentane hydrogenolysis activity compared to Pd.[38,58] In addition, CO does not bind to Au under the conditions of the chemisorption experiment; the temperature is too high, enabling the number of Pd surface atoms to be determined.[39,40] Increasing the weight loading of palladium also increases the particle size determined by chemisorption since more of the Au nanoparticle surface will be covered by Pd. The increase in Pd surface composition results in a decrease in isomerization selectivity to the extent that the 4% Pd–3.5% Au catalyst performs almost identically to the monometallic Pd (2.5 nm) catalyst. This behavior indicates gold must be in close contact to the surface palladium to influence the catalysis.

4.2 Comparison of geometric and electronic effects

Fig. 5a shows the dispersion determined by chemisorption for the pure Pd catalyst from our previous study combined with the PdAu selectivity data.[12] The monometallic Pd catalyst behavior was determined to be governed by electronic effects rather than changes in particle size as seen by the lack of a strong correlation in Fig. 5a. The figure demonstrates the addition of gold alters the behavior of palladium when it is in direct contact with the surface palladium. A similar sized monometallic palladium catalyst (by STEM) has an isomerization selectivity of 3% compared to the 0.52% Pd–3% Au catalyst which has a selectivity of 26%. Fig. 5b shows the heat of adsorption behavior for both Pd and PdAu catalysts. As the wt.% of Pd in the Pd/Au catalysts is increased, the measured CO heat of adsorption approaches that of pure Pd. The 4% Pd–3.5% Au catalyst has a heat of adsorption that fits well with our correlation from previous work, suggesting that the catalyst adsorbs CO more like Pd as the amount of added Pd increases.[12] Ward *et al.* found the heat of adsorption of CO did not change significantly when Pd was alloyed with Au.[39] The small changes were attributed to electronic effects through electron transfer from Pd to Au; however, the differences in heats of adsorption were not larger than the standard deviation given in their data. Neurock *et al.* performed a theoretical study of PdAu for ethylene hydrogenation and found the electronic effect due to rehybridization was

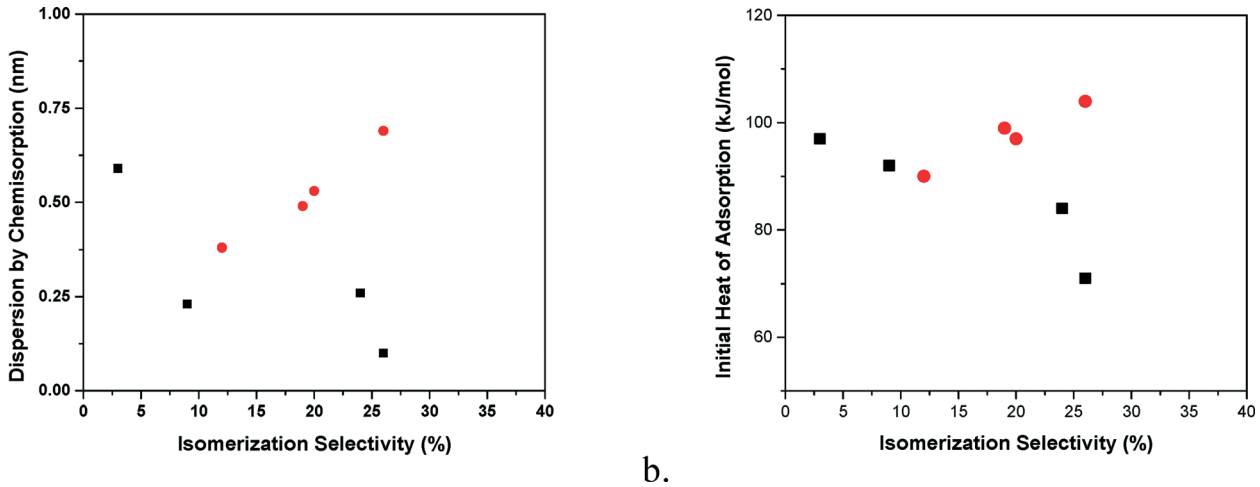

Fig. 5 a) Isomerization selectivity *vs.* particle size determined by CO chemisorption and b) initial CO heat of adsorption *vs.* isomerization selectivity of monometallic Pd (black squares) and PdAu (red circles) catalysts.

negligible compared to the contribution from geometric effects caused by the weakening of carbon and hydrogen bonding to Au.[34] Both figures suggest the gold must be close to the surface to have an effect on the catalytic performance and that the composition of the core of the particle is not important if the shell is thick enough to be contiguous, enabling the bimetallic particle to function as a monometallic nanoparticle.

The expansion of the Pd–Pd lattice seen in EXAFS may explain the changes in reactivity since the expansion may influence the adsorption configuration of neopentane. As suggested by Anderson and Avery, the adsorption of neopentane may require multi-site attachment to contiguous Pd atoms.[59] Changes in the bond distance between Pd atoms may affect the strength of neopentane adsorption to the surface or the ability of the surface to perform C–H and C–C bond cleaving reactions. The reduction in hydrogenolysis product selectivity would explain the increase in isomerization selectivity and the similarity of the turnover rate for neopentane disappearance due to the loss of ensembles for C–H and C–C bond cleavage. Although the performance of Pd has not been improved significantly by the addition of Au, two catalysts were created (the 3.0 nm Pd and the 0.52% Pd–3% Au) with significantly different surface bonding characteristics but very similar isomerization selectivity. This data also highlights the influence of the near-surface composition compared to the bulk properties of a nanoparticle on the catalytic performance.[60] The presence of gold alters the behavior of palladium relative to a monometallic nanoparticle with a similar effective diameter, however, the further the gold is from the catalyst surface the effect on the catalyst performance is lessened such that the 4% Pd–3.5% Au catalyst performs like pure Pd.

Corner and edge sites typically bind adsorbates more strongly and are more active for bond-breaking reactions compared to terrace sites.[61–63] To interrogate the types of sites available, CO adsorption on these catalysts monitored by DRIFTS has been used. The addition of gold decreases the amount of bridge-bound CO as seen in Fig. 4, which could indicate an increase in the fraction of low coordination corner and edge sites. From previous work, Pd catalysts with low linear-to-bridge ratios resulted in higher isomerization selectivity,[12] but the PdAu catalysts do not follow this trend as the 0.52% Pd–3% Au and 1% Pd–3% Au catalysts had the highest linear-to-bridge ratio and the highest isomerization selectivity of all catalysts. Both these catalysts have an isomerization selectivity similar to the largest Pd particles tested in our previous work; however, the linear-to-bridge ratios are significantly different. The best Pd catalysts in terms of isomerization selectivity had a linear-to-bridge ratio of ~0.15 : 1 while the PdAu catalysts with similar selectivity behavior have a ratio of 0.59 : 1 (0.52% Pd–3% Au) and 0.94 : 1 (1% Pd–3% Au).[12] Fig. 6 shows the isomerization and hydrogenolysis turnover rates *versus* the linear-to-bridge ratio for the PdAu catalysts. The neopentane hydrogenolysis rate decreases with increasing linear bound CO while the isomerization rate is insensitive to

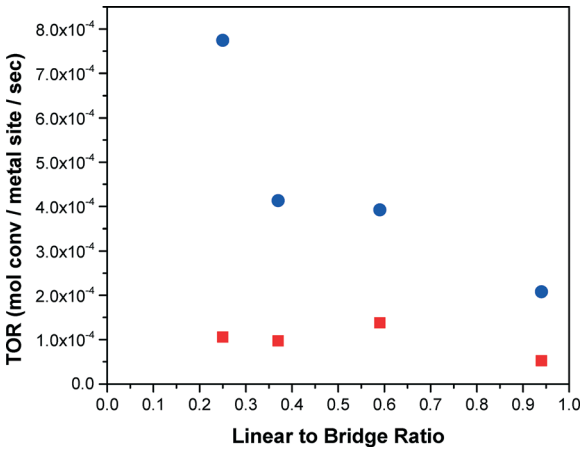

Fig. 6 Hydrogenolysis (blue circles) and isomerization (red squares) turnover rate *versus* the linear to bridge ratio from DRIFTS of CO adsorption.

changes in surface structure. As mentioned above, hydrogenolysis is a well-known structure-sensitive reaction which requires a minimum ensemble of two active sites.[64–66] The increase in linear bound CO suggests that large Pd ensembles are broken up by Au. Although our previous work with neopentane conversion suggests that the active site for hydrogenolysis and isomerization are similar, apparently, the presence of Au does not prevent formation of the transition state for isomerization. This suggests that the hydrogenolysis activity is altered by geometric effects although the overall neopentane conversion activity is not greatly affected.

Fig. 7 shows the relationship between neopentane isomerization selectivity compared to the surface structure assessed by DRIFTS. Decreasing bridge bound CO results in an increase in isomerization selectivity but this effect appears to reach a maximum at around 0.55 where the selectivity levels off. This suggests that breaking up large Pd ensembles on the surface is desirable, but limited as an approach to increase isomerization selectivity.

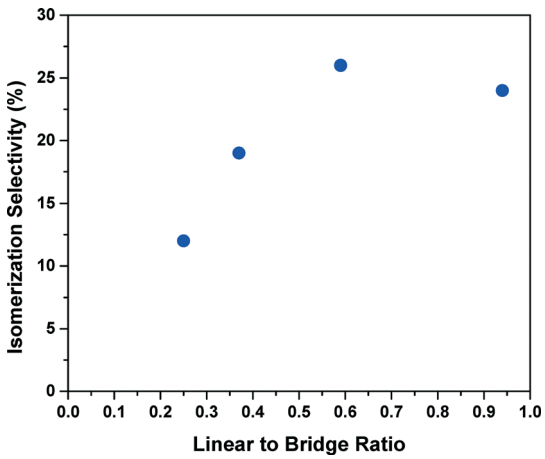

Fig. 7 Linear-to-bridge ratio from DRIFTS of CO adsorption *vs.* isomerization selectivity for PdAu catalysts.

5.0 Conclusion

Alloying palladium with gold on a silica support to form a Pd(shell)–Au(core) nanoparticle improved the neopentane isomerization selectivity compared to a silica-supported monometallic palladium catalyst with a similar particle size. This improvement was more significant when the Pd shell was influenced by the underlying Au core (*i.e.*, lower Pd weight loading catalysts). As the amount of palladium added to the catalyst increased, the catalytic behavior was similar to monometallic Pd. The turnover rate for hydrogenolysis decreased as the fraction of Au increased which correlated with an increase CO linear-to-bridge ratio. Calorimetry showed that the electronic effect of Au addition lessened with increasing Pd wt.%. Although both electronic and geometric effects have been observed, the changes in catalytic performance correlate more with changes in geometry. The identity of the metal atoms in the core of the particle appears to be less significant to catalytic properties than the surface composition and metal atoms near the surface.

Acknowledgements

JTM and NS were supported as part of the Institute for Atom-Efficient Chemical Transformations (IACT), an Energy Frontier Research Center funded by the U.S. Department of Energy, Office of Science, Office of Basic Energy Sciences. R. J. M. and D. C. gratefully acknowledge funding for this work from the National Science Foundation (CBET grant no. 0747646). Partial funding for DC was provided by the Chemical Sciences and Engineering Division at Argonne National Laboratory and the Office of the Vice Chancellor for Research at the University of Illinois at Chicago. S. M. K. S. and R. M. R. acknowledge funding from the Department of Energy, Office of Basic Energy Sciences, Chemical Sciences, Geosciences, and Biosciences Division, Catalysis Sciences Program under grant number DE-FG02-12ER16364. R. M. R. acknowledges financial support provided through a 3M Non-Tenured Faculty Grant (NTFG). The STEM work was performed at the UIC Research Resource Center. Use of the Advanced Photon Source was supported by the U.S. Department of Energy, Office of Science, Office of Basic Energy Sciences, under contract no. DE-AC02-06CH11357. MRCAT operations are supported by the Department of Energy and the MRCAT member institutions. The CleanCat Core facility acknowledges funding from the Department of Energy (DE-FG02-03ER15457 and DE-AC02-06CH11357) used for the purchase of the DRIFTS system and the AMI-200, respectively.

References

1 J. A. Rodriguez and D. W. Goodman, *J. Phys. Chem.*, 1991, **95**, 4196–4206.
2 J. A. Rodriguez and D. W. Goodman, *Science*, 1992, **257**, 897–903.
3 J. H. Sinfelt, *Sci. Am.*, 1985, **253**, 90–98.
4 K. Balakrishnan and J. Schwank, *J. Catal.*, 1991, **132**, 451–464.
5 T. P. Wu, D. J. Childers, C. Gomez, A. M. Karim, N. M. Schweitzer, A. J. Kropf, H. Wang, T. B. Bolin, Y. F. Hu, L. Kovarik, R. J. Meyer and J. T. Miller, *ACS Catal.*, 2012, **2**, 2433–2443.
6 A. Gross, *Top. Catal.*, 2006, **37**, 29–39.
7 J. Sehested, K. E. Larsen, A. L. Kustov, A. M. Frey, T. Johannessen, T. Bligaard, M. P. Andersson, J. K. Norskov and C. H. Christensen, *Top. Catal.*, 2007, **45**, 9–13.
8 B. Hammer and J. K. Norskov, *Surf. Sci.*, 1995, **343**, 211–220.
9 B. Hammer and J. K. Norskov, Impact of Surface Science on Catalysis, in *Advances in Catalysis*, ed. B. C. Gates and H. Knozinger, 2000, vol. 45, pp. 71–129.
10 J. Kleis, J. Greeley, N. A. Romero, V. A. Morozov, H. Falsig, A. H. Larsen, J. Lu, J. J. Mortensen, M. Dulak, K. S. Thygesen, J. K. Norskov and K. W. Jacobsen, *Catal. Lett.*, 2011, **141**, 1067–1071.
11 N. Schweitzer, H. L. Xin, E. Nikolla, J. T. Miller and S. Linic, *Top. Catal.*, 2010, **53**, 348–356.
12 D. Childers, A. Saha, N. Schweitzer, R. M. Rioux, J. T. Miller and R. J. Meyer, *ACS Catal.*, 2013, **3**, 2487–2496.
13 F. Gao and D. W. Goodman, *Chem. Soc. Rev.*, 2012, **41**, 8009–8020.
14 J. Rebelli, A. A. Rodriguez, S. G. Ma, C. T. Williams and J. R. Monnier, *Catal. Today*, 2011, **160**, 170–178.
15 M. Bonarowska, J. Pielaszek, W. Juszczyk and Z. Karpinski, *J. Catal.*, 2000, **195**, 304–315.
16 P. Dash, T. Bond, C. Fowler, W. Hou, N. Coombs and R. W. J. Scott, *J. Phys. Chem. C*, 2009, **113**, 12719–12730.
17 N. El Kolli, L. Delannoy and C. Louis, *J. Catal.*, 2013, **297**, 79–92.
18 A. M. Venezia, L. F. Liotta, G. Pantaleo, V. La Parola, G. Deganello, A. Beck, Z. Koppany, K. Frey, D. Horvath and L. Guczi, *Appl. Catal., A*, 2003, **251**, 359–368.
19 A. Sarkany, O. Geszti and G. Safran, *Appl. Catal., A*, 2008, **350**, 157–163.
20 K. Luo, T. Wei, C. W. Yi, S. Axnanda and A. W. Goodman, *J. Phys. Chem. B*, 2005, **109**, 23517–23522.
21 S. W. T. Price, J. M. Rhodes, L. Calvillo and A. E. Russell, *J. Phys. Chem. C*, 2013, **117**, 24858–24865.
22 A. F. Lee, C. J. Baddeley, C. Hardacre, R. M. Ormerod, R. M. Lambert, G. Schmid and H. West, *J. Phys. Chem.*, 1995, **99**, 6096–6102.
23 M. S. Chen, D. Kumar, C. W. Yi and D. W. Goodman, *Science*, 2005, **310**, 291–293.
24 X. Yang, C. Huang, Z. Y. Fu, H. Y. Song, S. J. Liao, Y. L. Su, L. Du and X. J. Li, *Appl. Catal., B*, 2013, **140**, 419–425.
25 P. Dolle, R. Baudoing-Savois, M. De Santis, M. C. Saint-Lager, M. Abel, J. C. Bertolini and P. Delichère, *Surf. Sci.*, 2002, **518**, 1–13.
26 Z. Li, F. Gao, O. Furlong and W. T. Tysoe, *Surf. Sci.*, 2010, **604**, 136–143.
27 B. Zhu, G. Thrimurthulu, L. Delannoy, C. Louis, C. Mottet, J. Creuze, B. Legrand and H. Guesmi, *J. Catal.*, 2013, **308**, 272–281.

28 F. Gao, Y. L. Wang and D. W. Goodman, *J. Phys. Chem. C*, 2009, **113**, 14993–15000.
29 G. Mazzone, I. Rivalta, N. Russo and E. Sicilia, *J. Phys. Chem. C*, 2008, **112**, 6073–6081.
30 H. L. Abbott, A. Aumer, Y. Lei, C. Asokan, R. J. Meyer, M. Sterrer, S. Shaikhutdinov and H. J. Freund, *J. Phys. Chem. C*, 2010, **114**, 17099–17104.
31 V. Soto-Verdugo and H. Metiu, *Surf. Sci.*, 2007, **601**, 5332–5339.
32 D. Yuan, X. Gong and R. Wu, *Phys. Rev. B: Condens. Matter Mater. Phys.*, 2007, **75**, 233401.
33 T. Wei, J. Wang and D. W. Goodman, *J. Phys. Chem. C*, 2007, **111**, 8781–8788.
34 M. Neurock and D. H. Mei, *Top. Catal.*, 2002, **20**, 5–23.
35 M. Garcia-Mota and N. Lopez, *Phys. Rev. B: Condens. Matter Mater. Phys.*, 2010, **82**, 075411.
36 K. Balakrishnan and J. Schwank, *J. Catal.*, 1991, **132**, 451–464.
37 J. R. Regalbuto, *Catalyst Preparation: Science and Engineering*, CRC Press, 2006.
38 M. Boudart and L. D. Ptak, *J. Catal.*, 1970, **16**, 90–96.
39 T. Ward, L. Delannoy, R. Hahn, S. Kendell, C. J. Pursell, C. Louis and B. D. Chandler, *ACS Catal.*, 2013, **3**, 2644–2653.
40 F. Menegazzo, M. Manzoli, A. Chiorino, F. Boccuzzi, T. Tabakova, M. Signoretto, F. Pinna and N. Pernicone, *J. Catal.*, 2006, **237**, 431–434.
41 M. A. Vannice and C. C. Twu, *J. Chem. Phys.*, 1981, **75**, 5944–5948.
42 L. Bollmann, J. L. Ratts, A. M. Joshi, W. D. Williams, J. Pazmino, Y. V. Joshi, J. T. Miller, A. J. Kropf, W. N. Delgass and F. H. Ribeiro, *J. Catal.*, 2008, **257**, 43–54.
43 J. T. Miller, A. J. Kropf, Y. Zha, J. R. Regalbuto, L. Delannoy, C. Louis, E. Bus and J. A. van Bokhoven, *J. Catal.*, 2006, **240**, 222–234.
44 M. R. Knecht, M. G. Weir, A. I. Frenkel and R. M. Crooks, *Chem. Mater.*, 2008, **20**, 1019–1028.
45 T. Lear, R. Marshall, J. A. Lopez-Sanchez, S. D. Jackson, T. M. Klapotke, M. Baumer, G. Rupprechter, H. J. Freund and D. Lennon, *J. Chem. Phys.*, 2006, 124.
46 J. L. Lu, B. S. Fu, M. C. Kung, G. M. Xiao, J. W. Elam, H. H. Kung and P. C. Stair, *Science*, 2012, **335**, 1205–1208.
47 A. Hugon, L. Delannoy, J.-M. Krafft and C. Louis, *J. Phys. Chem. C*, 2010, **114**, 10823–10835.
48 J. B. Giorgi, T. Schroeder, M. Baumer and H. J. Freund, *Surf. Sci.*, 2002, **498**, L71–L77.
49 J. S. Bradley, E. W. Hill, S. Behal, C. Klein, B. Chaudret and A. Duteil, *Chem. Mater.*, 1992, **4**, 1234–1239.
50 S. Marx, F. Krumeich and A. Baiker, *J. Phys. Chem. C*, 2011, **115**, 8195–8205.
51 A. M. Venezia, V. La Parola, G. Deganello, B. Pawelec and J. L. G. Fierro, *J. Catal.*, 2003, **215**, 317–325.
52 G. Rupprechter, M. Morkel, H. J. Freund and R. Hirschl, *Surf. Sci.*, 2004, **554**, 43–59.
53 W. Y. Yu, G. M. Mullen and C. B. Mullins, *J. Phys. Chem. C*, 2014, **118**, 2129–2137.
54 W. Y. Yu, G. M. Mullen and C. B. Mullins, *J. Phys. Chem. C*, 2013, **117**, 19535–19543.
55 M. E. Bjorketun, G. S. Karlberg, J. Rossmeisl, I. Chorkendorff, H. Wolfschmidt, U. Stimming and J. K. Norskov, *Phys. Rev. B: Condens. Matter Mater. Phys.*, 2011, **84**, 045407.
56 N. A. Bhore, M. T. Klein and K. B. Bischoff, *Ind. Eng. Chem. Res.*, 1990, **29**, 313–316.
57 T. Akita, T. Hiroki, S. Tanaka, T. Kojima, M. Kohyama, A. Iwase and F. Hori, *Catal. Today*, 2008, **131**, 90–97.
58 W. Juszczyk, D. Lomot, Z. Karpinski and J. Pielaszek, *Catal. Lett.*, 1995, **31**, 37–45.
59 J. R. Anderson and N. R. Avery, *J. Catal.*, 1966, **5**, 446–463.
60 J. Greeley and M. Mavrikakis, *Nat. Mater.*, 2004, **3**, 810–815.
61 B. Hammer, *Top. Catal.*, 2006, **37**, 3–16.
62 S. Dahl, A. Logadottir, R. C. Egeberg, J. H. Larsen, I. Chorkendorff, E. Tornqvist and J. K. Norskov, *Phys. Rev. Lett.*, 1999, **83**, 1814–1817.
63 R. C. Egeberg, S. Dahl, A. Logadottir, J. H. Larsen, J. K. Norskov and I. Chorkendorff, *Surf. Sci.*, 2001, **491**, 183–194.
64 D. W. Blakely and G. A. Somorjai, *J. Catal.*, 1976, **42**, 181–196.
65 D. W. Flaherty, D. D. Hibbitts, E. I. Gürbüz and E. Iglesia, *J. Catal.*, 2014, **311**, 350–356.
66 J. H. Sinfelt, *CRC Crit. Rev. Solid State Sci.*, 1973, **4**, 311–332.